

Could k -NN classifier be useful in tree leaves recognition?

KATEŘINA HORAISOVÁ and JAROMÍR KUKAL

This paper presents a method for affine invariant recognition of two-dimensional binary objects based on 2D Fourier power spectrum. Such function is translation invariant and their moments of second order enable construction of affine invariant spectrum except of the rotation effect. Harmonic analysis of samples on circular paths generates Fourier coefficients whose absolute values are affine invariant descriptors. Affine invariance is approximately saved also for large digital binary images as demonstrated in the experimental part. The proposed method is tested on artificial data set first and consequently on a large set of 2D binary digital images of tree leaves. High dimensionality of feature vectors is reduced via the kernel PCA technique with Gaussian kernel and the k -NN classifier is used for image classification. The results are summarized as k -NN classifier sensitivity after dimensionality reduction. The resulting descriptors after dimensionality reduction are able to distinguish real contours of tree leaves with acceptable classification error. The general methodology is directly applicable to any set of large binary images. All calculations were performed in the MATLAB environment.

Key words: binary image, Fourier transform, affine invariance, harmonic analysis, pattern recognition, k -NN classifier

1. Introduction

Applications of computer vision enjoy greater attention recently. Cameras are used almost everywhere and their images are processed consequently. Many researchers try to create various systems which would consider one object taken from various places as same. Flusser and Suk [9] introduced the moment invariants, which are invariant against general affine transformation and may be used for recognition of affine-deformed objects. Later the same authors [17] published a general method of systematic derivation of affine moment invariants of any weights and orders, whereas each invariant is expressed by its generating graph. Ho and Yang [11] introduced a method for affine registration of 2D point sets using complex numbers. It is based on polynomials with complex coefficients whose roots are the points in a given point set. Yang et al. [22] converted an object into a closed curve which is called radial centroid curve. The affine invariant

The Authors are with Czech Technical University in Prague, Faculty of Nuclear Sciences and Physical Engineering, Trojanova 13, Prague, Czech Republic, e-mail: katerina.horaisova@fjfi.cvut.cz

Received 2.09.2013. Revised 18.03.2014.

function is constructed by applying a stationary wavelet transform to the derived curve. In another paper [23] they constructed the affine invariant functions directly in spatial domain, on the object contour without any transformation. They also introduced cutting affine moment invariants [24]. The original image is cut into two areas by a closed curve called general contour. Then the traditional affine moment invariants method is applied to the new image, which is obtained by changing gray value of pixels in the inside area. Sheta et al. [15] proposed the fuzzy system for 3D objects recognition based on 2D images. They used the fuzzy mathematical model of the extracted features for the classification.

There was a rapid increase in the size of digital image collections in recent years. Therefore, content-based image retrieval [16] has become one of the most developed field of computer vision for image retrieval [5, 13, 19]. Image retrieval system provides the most similar images from a given database when the query image is submitted. Many researchers deal with shape retrieval from binary image databases containing for example botanical collections [4, 7, 14, 20, 21], medical images [2, 3], road signs [8], trademarks [12], or patent images [18].

This paper presents novel method for constructing affine invariant descriptors based on 2D Fourier transform. The method consists of three steps. First we convert the original image to its power spectrum. Then we used image moments to obtain affine invariant spectrum except effect of second rotation. The novelty of our approach is the third step, when we analyze 1D signal produced by circular motion around origin in frequency domain. The method is derived in the continuous space domain in Sect. 2 and extended to digital binary images in Sect. 2.1. The terms of generalized sensitivity and compromise sensitivity are introduced in Sect. 3. The properties of affine invariant descriptors are experimentally verified on artificial images and consequently on real digital images of tree leaves in Sect. 4. The k -NN classifier is used for classification.

2. Affine invariant system

First we define normalized 2D power spectrum as

$$\Phi(\omega_1, \omega_2) = \left| \frac{F(\omega_1, \omega_2)}{F(0, 0)} \right|^2 \quad (1)$$

for non-empty image, where F denotes continuous 2D Fourier transform. Function Φ is invariant to any translation of 2D image. Let $p, q \in \mathbb{N}_0$ be orders. Then image moments [10] are defined as

$$m_{p,q} = \int_0^N \int_0^N x_1^p x_2^q f(x_1, x_2) dx_1 dx_2 \quad (2)$$

and modified central moments of 2^{nd} order are for an non-empty image defined as

$$\mu_{2,0} = \frac{m_{2,0}}{m_{0,0}} - \left(\frac{m_{1,0}}{m_{0,0}} \right)^2, \quad (3)$$

$$\mu_{1,1} = \frac{m_{1,1}}{m_{0,0}} - \frac{m_{1,0}}{m_{0,0}} \frac{m_{0,1}}{m_{0,0}}, \quad (4)$$

$$\mu_{0,2} = \frac{m_{0,2}}{m_{0,0}} - \left(\frac{m_{0,1}}{m_{0,0}} \right)^2. \quad (5)$$

The matrix

$$G = \begin{pmatrix} \mu_{2,0} & \mu_{1,1} \\ \mu_{1,1} & \mu_{0,2} \end{pmatrix} \quad (6)$$

is positive definite with eigenvalues $\lambda_1 \geq \lambda_2 > 0$ and eigenvectors \vec{e}_1, \vec{e}_2 .

Now, the second order approximation of 2D power spectrum is

$$\Phi(\omega_1, \omega_2) \approx 1 - \mu_{2,0}\omega_1^2 - 2\mu_{1,1}\omega_1\omega_2 - \mu_{0,2}\omega_2^2. \quad (7)$$

The spectrum is radially symmetric just when $\mu_{2,0} = \mu_{0,2}$ and $\mu_{1,1} = 0$. To guarantee the radial symmetry of a new spectrum, we use eigenvalue decomposition (EVD) of matrix G and calculate transformation matrix

$$A = (\vec{e}_1 | \vec{e}_2) \begin{pmatrix} \lambda_1^{-\frac{1}{2}} & 0 \\ 0 & \lambda_2^{-\frac{1}{2}} \end{pmatrix}. \quad (8)$$

It is easy to construct radially symmetric 2D spectrum

$$\Psi(\omega_1, \omega_2) = \Phi(A\vec{\omega}) = \Phi(a_{1,1}\omega_1 + a_{1,2}\omega_2, a_{2,1}\omega_1 + a_{2,2}\omega_2) \quad (9)$$

from the power spectrum and matrix A . The second order approximation is then

$$\Psi(\omega_1, \omega_2) \approx 1 - \omega_1^2 - \omega_2^2. \quad (10)$$

The 2D spectrum Ψ is invariant to both translation and scaling. It is also well prepared for the construction of affine invariant system. We can use polar coordinates for $\omega \geq 0$ and $\varphi \in [0, 2\pi]$. Function $\Psi(\omega \cos \varphi, \omega \sin \varphi)$ is periodic in φ with period π for any fixed ω . Thus, the function can be expressed as Fourier series for the given ω . The squared absolute values of Fourier coefficients are

$$C_n(\omega) = \left| \frac{1}{\pi} \int_0^\pi \Psi(\omega \cos \varphi, \omega \sin \varphi) e^{-2in\varphi} d\varphi \right|^2 \quad (11)$$

for $n \in \mathbb{N}_0$, $\omega \geq 0$. Functions $C_n(\omega)$ are affine invariant with respect to changes in 2D image f and enable to recognize 2D binary objects.

2.1. Discrete case

In discrete case we can use the relationship between spectrum $F(\omega_1, \omega_2)$ and its discrete analogy $F^+(\omega_1, \omega_2)$. Therefore, we obtained

$$|F(\omega_1, \omega_2)| \approx \left| \frac{\sin \frac{\omega_1}{2}}{\frac{\omega_1}{2}} \right| \left| \frac{\sin \frac{\omega_2}{2}}{\frac{\omega_2}{2}} \right| |F^+(\omega_1, \omega_2)|. \quad (12)$$

This approximation enables to make another Taylor expansion of 2^{nd} order

$$\Phi(\omega_1, \omega_2) \approx 1 - \left(\mu_{2,0}^+ + \frac{1}{12} \right) \omega_1^2 - 2\mu_{1,1}^+ \omega_1 \omega_2 - \left(\mu_{0,2}^+ + \frac{1}{12} \right) \omega_2^2, \quad (13)$$

where

$$m_{p,q}^+ = \sum_{k_1=0}^{N-1} \sum_{k_2=0}^{N-1} k_1^p k_2^q f^+(k_1, k_2), \quad (14)$$

$$\mu_{2,0}^+ = \frac{m_{2,0}^+}{m_{0,0}^+} - \left(\frac{m_{1,0}^+}{m_{0,0}^+} \right)^2, \quad (15)$$

$$\mu_{1,1}^+ = \frac{m_{1,1}^+}{m_{0,0}^+} - \frac{m_{1,0}^+ m_{0,1}^+}{m_{0,0}^+ m_{0,0}^+}, \quad (16)$$

$$\mu_{0,2}^+ = \frac{m_{0,2}^+}{m_{0,0}^+} - \left(\frac{m_{0,1}^+}{m_{0,0}^+} \right)^2. \quad (17)$$

If the discrete image is non-empty, then image moment $m_{0,0}^+ > 0$ and matrix

$$G^+ = \begin{pmatrix} \mu_{2,0}^+ + \frac{1}{12} & \mu_{1,1}^+ \\ \mu_{1,1}^+ & \mu_{0,2}^+ + \frac{1}{12} \end{pmatrix} \quad (18)$$

is also positive definite with eigenvalues $\lambda_1^+ \geq \lambda_2^+ > 0$ and eigenvectors \vec{e}_1^+, \vec{e}_2^+ . In analogy with non-discrete case we obtained

$$A^+ = (\vec{e}_1^+ | \vec{e}_2^+) \begin{pmatrix} (\lambda_1^+)^{-\frac{1}{2}} & 0 \\ 0 & (\lambda_2^+)^{-\frac{1}{2}} \end{pmatrix}. \quad (19)$$

Now we can construct a discrete radially symmetric 2D spectrum from discrete normalized 2D power spectrum

$$\Phi^+(\omega_1, \omega_2) = \left(\frac{\sin \frac{\omega_1}{2}}{\frac{\omega_1}{2}} \frac{\sin \frac{\omega_2}{2}}{\frac{\omega_2}{2}} \right)^2 \left| \frac{F^+(\omega_1, \omega_2)}{F^+(0,0)} \right|^2, \quad (20)$$

as

$$\Psi^+(\omega_1, \omega_2) = \Phi^+(A^+\vec{\omega}) = \Phi^+(a_{1,1}^+\omega_1 + a_{1,2}^+\omega_2, a_{2,1}^+\omega_1 + a_{2,2}^+\omega_2). \quad (21)$$

Finally, we obtained discrete approximations

$$C_n^+(\omega) = \left| \frac{1}{\pi} \int_0^\pi \Psi^+(\omega \cos \varphi, \omega \sin \varphi) e^{-2in\varphi} d\varphi \right|^2 \quad (22)$$

for $n \in \mathbb{N}_0$, $\omega \geq 0$. It is clear that $C_n(\omega) \approx C_n^+(\omega)$, but $C_n^+(\omega)$ are not affine invariant functions. They are only good approximations of exact affine invariant functions $C_n(\omega)$.

3. Sensitivity and its generalization

Terms of sensitivity and specificity [1] are frequently used for evaluation of classification quality. For generalization to more classes it is sufficient to define the term of sensitivity. Let N be a number of classes, m_j be a number of patterns for the given class, and c_j be a count of correct classified patters for the given class. Then we define the sensitivity for j^{th} class as

$$se_j = \frac{c_j}{m_j}. \quad (23)$$

Then we can compute the compromise sensitivity as

$$Q = \left(\sum_{j=1}^N (1 - se_j)^p \right)^{\frac{1}{p}}, \quad (24)$$

specially, for $p = 1$ it is absolute distance from ideal alternative

$$AIA = \sum_{j=1}^N (1 - se_j). \quad (25)$$

Compromise sensitivity AIA will be used in the experimental part to choose the best k -NN classifier.

4. Experimental part

4.1. Experiments on artificial data

In order to illustrate potential of the proposed method, we carried out the following experimental study. We used the Mpeg7 CE-Shape-1 database [25], which consists of 70 classes with 20 images in each of them. Samples of database are depicted in Fig. 1.

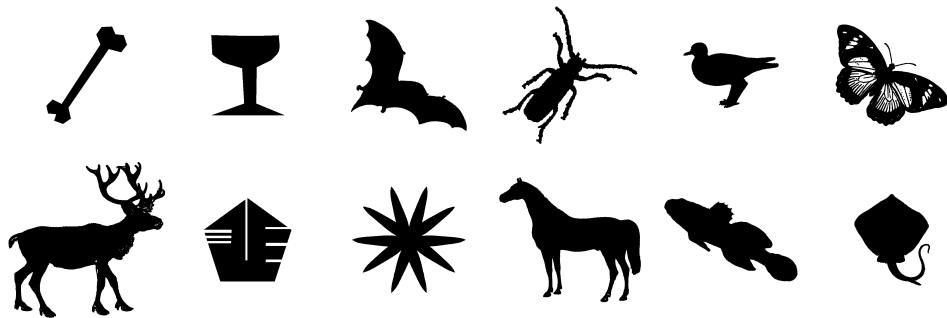


Figure 1. Sample images of CE-Shape-1 database.

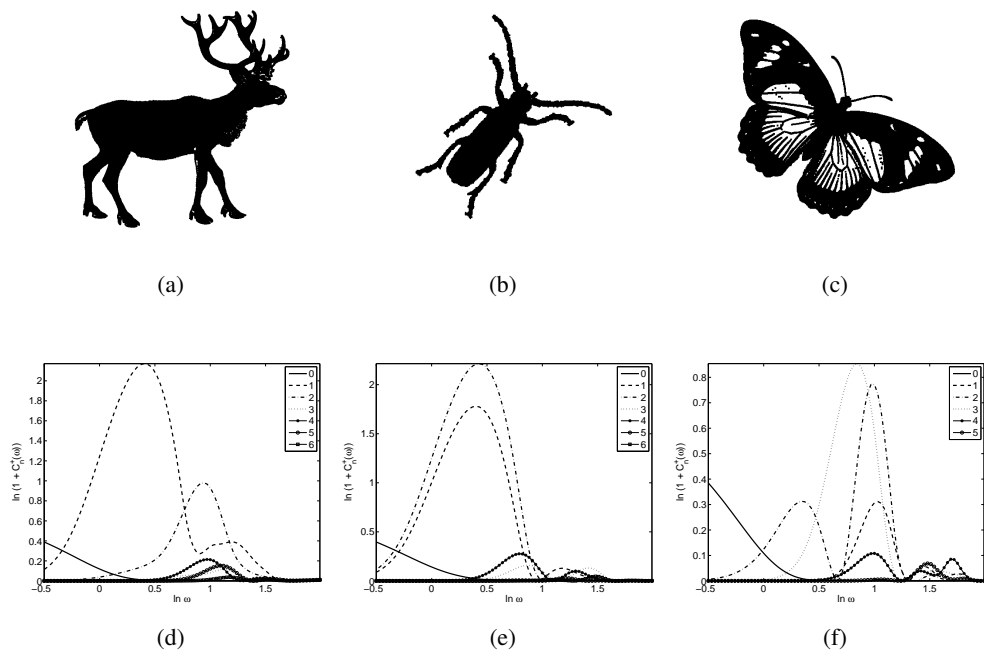


Figure 2. Harmonics for three objects.

In the first experiment the robustness of features to affine transform was studied. Our derived database of binary images includes one image from each class as etalon and 72 derived shapes from each etalon by affine transformations: translation with random shift $(x_0, y_0) \in \langle 0, 1 \rangle^2$, first rotation with angles $9^\circ, 36^\circ, 45^\circ, 90^\circ, 120^\circ$, and 150° , scaling with factors 0.33, 0.5 and 1.5, stretching with factors 1.5 and 2, and second rotation with angles 30° and 60° . Therefore, our database consists of 5110 binary images (70 etalons and 5040 transformed images).

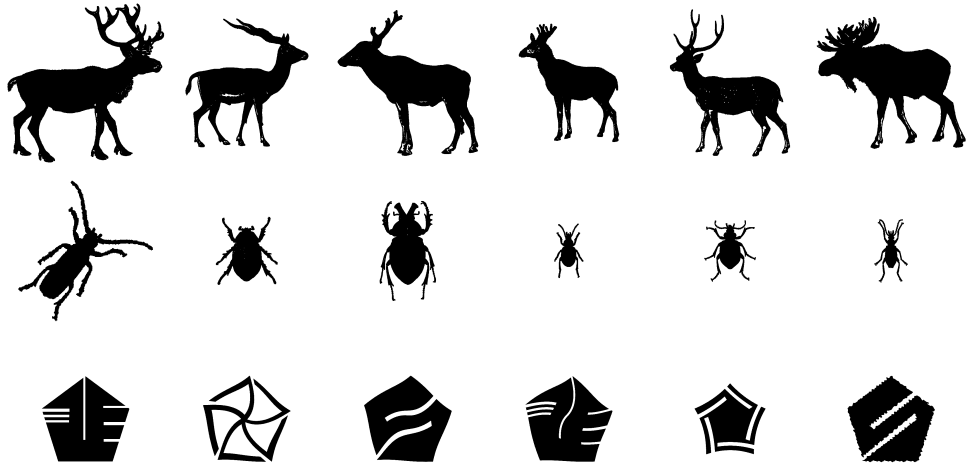


Figure 3. Samples within the same class.

The influence of etalon shape on harmonic frequencies is illustrated in Fig. 2, where harmonics for selected representatives are depicted. The number corresponds to the order of harmonic frequency. All harmonic frequencies (except $C_0(\omega)$) were 10000 times zoomed. Then, only the most significant harmonics (with the maximal value greater than 0.02) are depicted. Harmonics $C_n^+(\omega)$, for $n \in [1, 6]$ were used for classification with 26 samples per each harmonic. So, for each pattern, a 156-feature vector was created.

The k -nearest neighbor algorithm [6] was used for classification. We divided data to training and testing sets. The training set contained 70 feature vectors of etalons and the testing set contains 5040 feature vectors of transformed images. Except three images (small etalon of human transformed with scale factor 0.33) were all images classified correctly.

In the second experiment the ability of similar images recognition was tested. All 1400 images from CE-Shape-1 database were used. The variability of images within one class is demonstrated in Fig. 3. Shapes in each row belong to the same class. Firstly, the data set was randomly divided into two halves, one was used as a training set, and the other as a testing set. Consequently, one sample was used as a testing set and rest of the data set as a training set. It was repeated for all images in the data set. The k -nearest neighbor algorithm was used for classification. Because of high dimensionality, the kernel PCA method was applied to harmonics to obtain H principal components. We used the Gaussian kernel with a single parameter σ . The classification quality was measured by compromise sensitivity AIA for $k \in [1, 10]$ and $H \in [2, 20]$. For comparison was the k -NN classifier also applied to raw data without dimensionality reduction. The results are summarized in Tab. 16 for the half to half cross-validation approach ($\frac{1}{2} \times \frac{1}{2}$) and in Tab. 17 for leave-one-out cross-validation (one \times rest).

Table 16. Half to half cross-validation for CE-Shape-1

k	use of kernel PCA				raw data	
	AIA	$E[\%]$	H	σ	AIA	$E[\%]$
1	10.10	14.43	13	2×10^7	10.70	15.29
2	10.10	14.43	13	2×10^7	10.70	15.29
3	11.90	17.00	14	2.5×10^7	14.20	20.29
4	12.70	18.14	13	3×10^7	14.10	20.14
5	14.30	20.43	13	2×10^7	15.80	22.57
6	15.20	21.71	18	2×10^7	17.30	24.71
7	16.20	23.14	19	5.5×10^7	17.90	25.57
8	17.10	24.43	20	9×10^7	18.80	26.86
9	18.10	25.86	19	5.5×10^7	20.60	29.43
10	18.60	26.57	19	5.5×10^7	21.20	30.29

Table 17. Leave-one-out cross-validation for CE-Shape-1

k	use of kernel PCA				raw data	
	AIA	$E[\%]$	H	σ	AIA	$E[\%]$
1	9.45	13.50	13	3×10^3	10.15	14.50
2	9.45	13.50	13	3×10^3	10.15	14.50
3	12.00	17.14	17	1.5×10^7	13.00	18.57
4	12.15	17.36	15	7×10^7	13.80	19.71
5	13.40	19.14	19	5.5×10^7	15.70	22.43
6	13.80	19.71	14	3×10^7	15.90	22.71
7	15.60	22.29	17	5.5×10^7	17.10	24.43
8	15.80	22.57	14	3×10^7	17.70	25.29
9	17.25	24.64	14	3×10^7	18.60	26.57
10	17.60	25.14	15	5×10^7	19.20	27.43

Values in the second column represent minima of all AIA values obtained for various parameters σ and H in kernel PCA for the appropriate k -NN classifier. The percentage of

misclassified objects is denoted E and can be seen in the third column. For completeness, the number of principal components and parameter σ for the best classifier are included in the fourth and the fifth columns of tables. For comparison, values of AIA and E are presented also for raw data without dimensionality reduction in the last two columns of tables.

In both tests, 1-NN and 2-NN classifiers were able to correctly recognize at least 85.5% of samples and for 10-NN classifier recognized at least 73.5% of samples. With respect to high variability of shapes within the same class it is quite good result.

Table 18. Classes of leaves.

Index	Acronym	Tree name	Latin name
1	Gi	Ginkgo	Ginkgo Biloba
2	Ma	Maple	Acer Platanoides
3	Bi	Birch	Betula Pendula
4	Wi	Willow	Salix Fragilis
5	Be	Beech	Fagus Sylvatica
6	Po	Poplar	Populus Canadensis
7	Li	Lime	Tilia x Vulgaris
8	Oa	Oak	Quercus Robur
9	As	Aspen	Populus Tremula
10	Ch	Cherry	Prunus Avium

4.2. Real data experiment

Real tree leaves photographs were studied in the second part of experiments. Ten trees were chosen (Tab. 18) with ten various leaves for each of them. Images of these leaves were taken from nine views – one from the top and eight from various angles and distances. So, in each leaf class there are 90 objects. The binary images of class representatives are in Fig. 4.

The influence of leaf shape on harmonic frequencies is illustrated in Fig. 5. It depicts harmonics for selected leaf representatives. The influence of camera position on harmonics was also studied. The variance of harmonics amplitude is given by many factors. The main of them are given by the segmentation and binarization of images. So, we can observe differences between harmonics of the same leaf photographed at various angles and distances. This is demonstrated on a single oak leaf in Fig. 6. It is very interesting to study harmonics of various leaves from the same class. Harmonics for three patterns

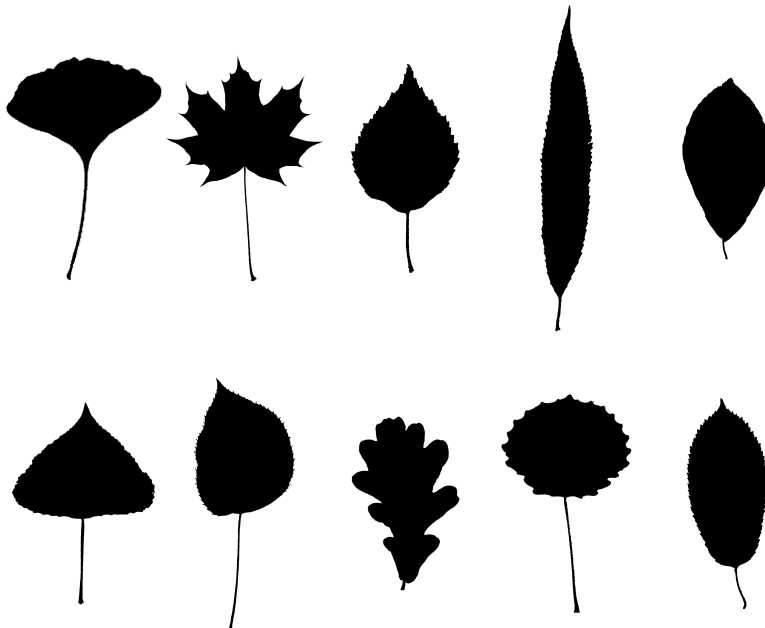


Figure 4. Classes representatives (ginkgo, maple, birch, willow, beech, poplar, lime, oak, aspen, and cherry).

from the oak class are depicted in Fig. 7. Although we can find differences in harmonics, the character and the shape of harmonics are the same.

There is time enough to finalize the process of classification using k -nearest neighbor algorithm. We again divided data to training and testing sets. The training set contained ten samples for each class (one sample for one leaf), in all the training set contained 100 feature vectors. The testing set contains the rest of data, so we had 800 testing feature vectors. Because of high dimensionality, the kernel PCA method was applied to harmonics to obtain H principal components as well as by artificial data experiment. The classification quality was measured by compromise sensitivity AIA for $k \in [1, 10]$ and $H \in [2, 20]$. For comparison was the k -NN classifier also applied to raw data without dimensionality reduction.

The results are summarized in Tab. 19. Inner values of table represent minimum of all AIA values obtained for various parameters σ in kernel PCA. Minimum AIA for given number of principal component (new data dimension) can be seen in appropriate line in the last column of table. This result is the best reached value cross all parameter σ values and all k -nearest neighbor classifiers and informs about ability of classification after given dimension reduction. The best k -NN classifier (for a given parameter k) was selected as the one with minimum compromise sensitivity AIA , which was used as criterion of classification quality. Its AIA is then presented in the last row of Tab. 19.

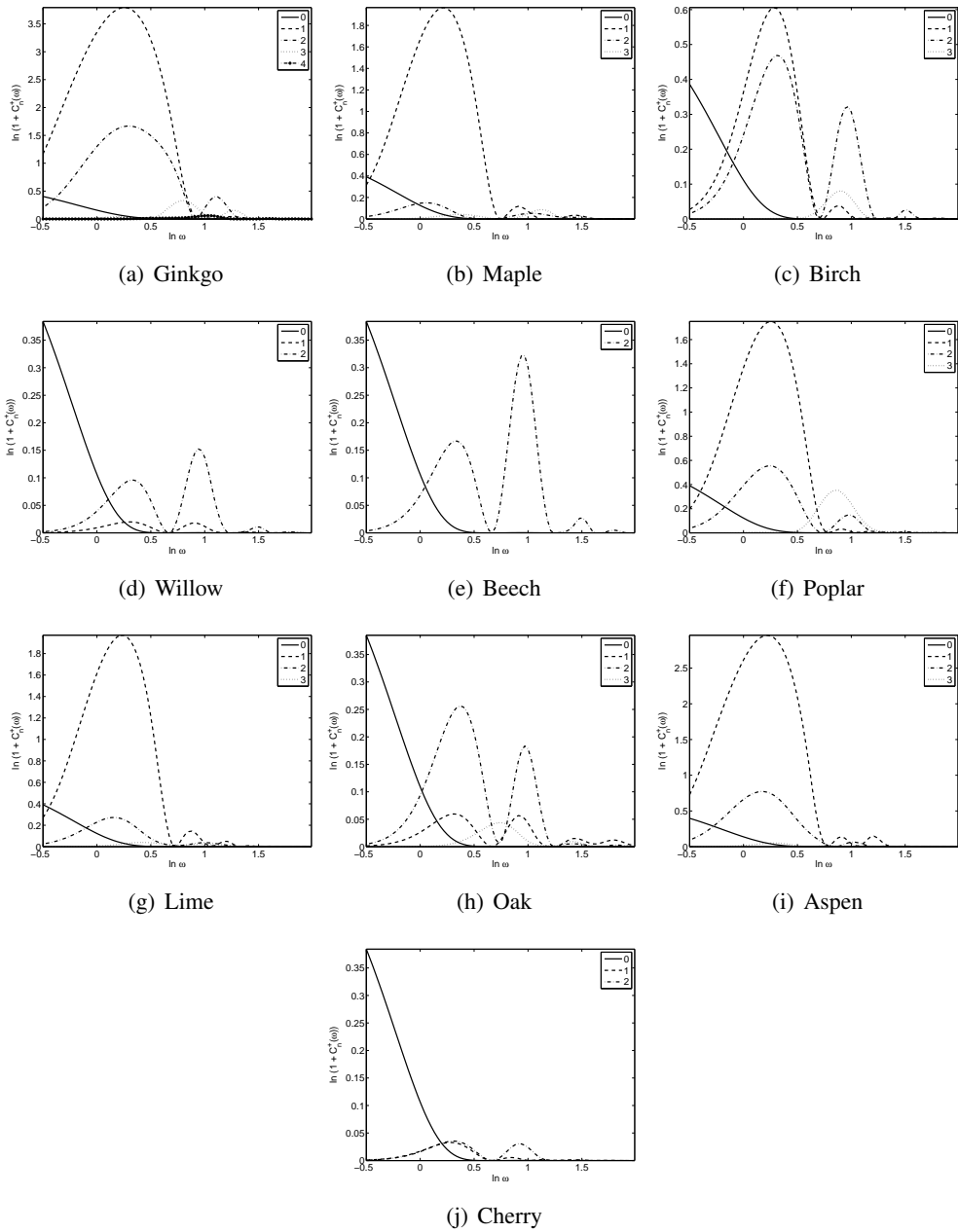


Figure 5. Harmonics for class representatives.

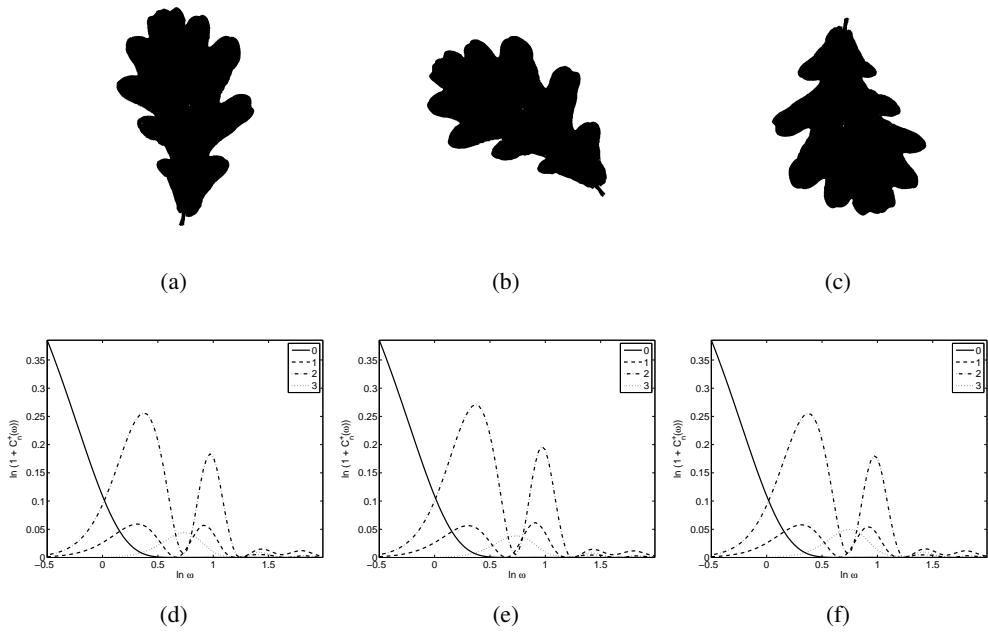


Figure 6. Single oak leaf photographs from various angles and distances.

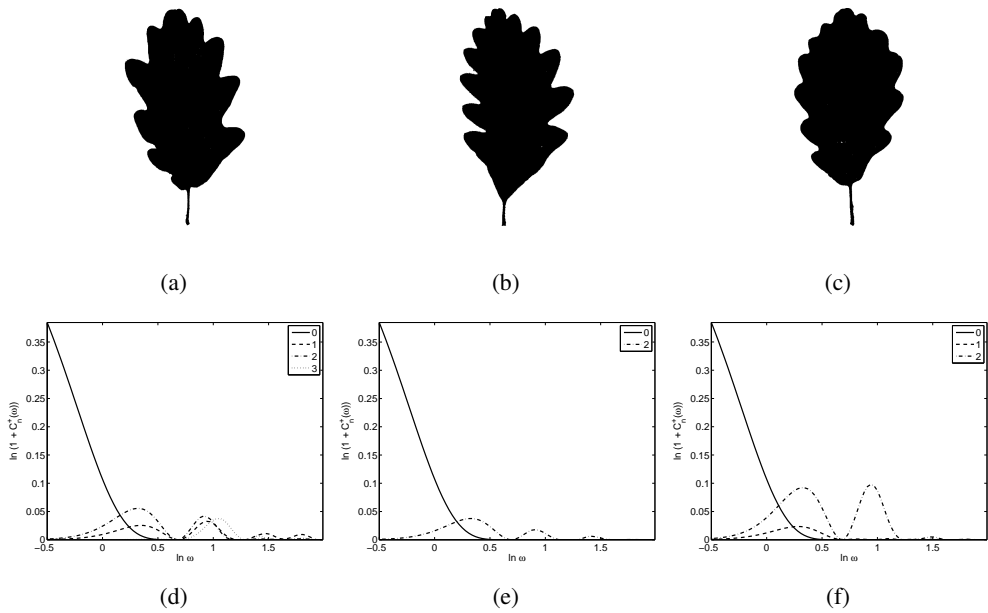


Figure 7. Sample patterns from the oak class.

Table 19. AIA of k -NN classifier after dimensionality reduction.

H	k										AIA_{\min}
	1	2	3	4	5	6	7	8	9	10	
2	2.14	2.14	2.45	2.21	2.41	2.50	2.59	2.75	2.85	3.21	2.14
3	0.88	0.88	1.35	1.54	1.75	1.75	1.94	1.89	2.03	2.09	0.88
4	0.50	0.50	1.08	1.21	1.42	1.56	1.64	1.65	1.76	1.81	0.50
5	0.21	0.21	0.72	0.75	0.96	0.85	1.05	1.02	1.41	1.39	0.21
6	0.15	0.15	0.57	0.49	0.72	0.59	0.84	0.81	0.84	0.84	0.15
7	0.05	0.05	0.49	0.39	0.54	0.52	0.80	0.72	0.84	0.81	0.05
8	0.04	0.04	0.47	0.44	0.55	0.44	0.81	0.79	0.99	1.10	0.04
9	0.05	0.05	0.67	0.61	0.98	0.76	1.00	0.93	1.11	1.06	0.05
10	0.05	0.05	0.64	0.59	0.86	0.75	0.92	0.92	1.02	1.05	0.05
11	0.07	0.07	0.65	0.57	0.89	0.80	0.97	1.02	1.10	1.24	0.07
12	0.07	0.07	0.61	0.61	0.79	0.84	0.96	1.00	1.10	1.19	0.07
13	0.05	0.05	0.67	0.57	0.77	0.85	0.92	0.95	1.13	1.17	0.05
14	0.04	0.04	0.56	0.55	0.85	0.85	0.88	1.01	1.06	1.11	0.04
15	0.05	0.05	0.60	0.65	0.86	0.79	0.96	1.09	1.15	1.21	0.05
16	0.05	0.05	0.56	0.66	0.79	0.76	0.88	0.96	1.01	1.14	0.05
17	0.05	0.05	0.47	0.55	0.68	0.69	0.79	0.89	1.07	1.12	0.05
18	0.01	0.01	0.34	0.49	0.65	0.65	0.74	0.91	0.95	1.14	0.01
19	0.02	0.02	0.29	0.40	0.66	0.70	0.84	0.90	1.05	1.11	0.02
20	0.05	0.05	0.25	0.40	0.68	0.81	0.84	0.90	1.06	1.21	0.05
raw	0.06	0.06	0.54	0.60	0.75	0.74	0.87	1.15	1.20	1.30	0.06
AIA_{\min}	0.01	0.01	0.25	0.39	0.54	0.44	0.74	0.72	0.84	0.81	

Corresponding sensitivities of classes for given k -NN classifier are summarized in Tab. 20. The percentage of misclassified objects is denoted E and can be seen in the last column of Tab. 20. For 1-NN and 2-NN classifier only one willow leaf was misclassified as beech. They both use kernel PCA to 18 principal components with $\sigma = 15 \times 10^6$. For 3-NN classifier, only 2.5 % of leaves were misclassified, namely as ginkgo, willow, lime, oak, and cherry classes. The generalized sensitivity was at least 0.86.

Table 20. Sensitivity of k -NN classifier.

k	Sensitivity of classes										se_{\min}	$E[\%]$
	se_1	se_2	se_3	se_4	se_5	se_6	se_7	se_8	se_9	se_{10}		
1	1.00	1.00	1.00	0.99	1.00	1.00	1.00	1.00	1.00	1.00	0.99	0.12
2	1.00	1.00	1.00	0.99	1.00	1.00	1.00	1.00	1.00	1.00	0.99	0.12
3	0.94	1.00	1.00	0.86	1.00	1.00	0.99	0.97	1.00	0.99	0.86	2.50
4	0.90	1.00	0.99	0.96	1.00	1.00	0.95	0.93	1.00	0.89	0.89	3.87
5	0.90	1.00	1.00	0.85	1.00	1.00	0.94	0.88	1.00	0.90	0.85	5.37
6	0.90	1.00	0.99	0.89	0.99	1.00	1.00	0.90	1.00	0.90	0.89	4.37
7	0.90	0.96	1.00	0.66	1.00	0.97	0.88	0.90	1.00	0.99	0.66	7.37
8	0.90	1.00	1.00	0.68	1.00	0.99	0.96	0.90	1.00	0.85	0.68	7.25
9	0.90	1.00	1.00	0.70	0.99	0.95	0.96	0.86	1.00	0.80	0.70	8.38
10	0.90	1.00	1.00	0.74	0.96	0.96	0.97	0.82	1.00	0.82	0.74	8.13

5. Conclusion

The affine invariant system of 2D binary image descriptors was developed. Its properties were derived in the continuous space domain and experimentally verified on artificial data first and consequently on real digital images of tree leaves. Used 1-NN or 2-NN classifier can be useful tool in tree leaves recognition, because the resulting descriptors after dimensionality reduction by kernel PCA are able to distinguish real contours of tree leaves with a classification error less than 0.2 % and generalized sensitivity at least 99 %. The general methodology is directly applicable to any set of large binary images.

References

- [1] D.G. ALTMAN and J. M. BLAND: Statistics Notes: Diagnostic tests 1: sensitivity and specificity. *British Medical J.*, **308**(6943), (1994), 1552.
- [2] S. ANTANI, L.R. LONG and G.R. THOMA: A biomedical information system for combined content-based retrieval of spine X-ray images and associated text information. *Proc. of the Indian Conf. on Computer Vision, Graphics, and Image Processing*, (2002), 16-21.
- [3] S. ANTANI, L.R. LONG and G.R. THOMA: Content-based image retrieval for large biomedical image archives. *Proc. of 11th World Congress on Medical Infor-*

- matics*, (2004), 829-833.
- [4] G. BORDOGNA, L. GHILARDI, S. MILESI and M. PAGANI: A Flexible System for the Retrieval of Shapes in Binary Images. *Applications of Fuzzy Sets Theory, Lecture Notes in Computer Science*, **4578** (2007), 370-377.
- [5] R. DATTA, D. JOSHI, J. LI and J.Z. WANG: Image retrieval: ideas, influences, and trends of the new age. *ACM Computing Surveys*, **40** (2008), 1-60.
- [6] R.O. DUDA, P.E. HART and D.G. STORK: Pattern Classification. Wiley Interscience, 2000.
- [7] J.-X. DU, X.-F. WANG and G.-J. ZHANG: Leaf shape based plant species recognition. *Applied Mathematics and Computation*, **185** (2007), 883-893.
- [8] P. DUKKIPATI and L. BROWN: Improving the recognition of geometrical shapes in road signs by augmenting the database. *Proc. of the Third Int. Conf. on Computer Science and its Applications*, (2005), 8-13.
- [9] J. FLUSSER and T. SUK: Pattern recognition by affine moment invariants. *Pattern Recognition*, **26**(1), (1993), 167-174.
- [10] R. GONZALES and R. WOODS: Digital Image Processing. Prentice-Hall, 2001.
- [11] J. HO and M. YANG: On affine registration of planar point sets using complex numbers. *Computer Vision and Image Understanding*, **115**(1), (2011), 50-58.
- [12] W.-Y. KIM and Y.-S. KIM: A region-based shape descriptor using Zernike moments. *Signal Processing: Image Communication*, **16** (2000), 95-102.
- [13] F. LONG, H. J. ZHANG and D.D. FENG: Fundamentals of content-based image retrieval. *Multimedia Information Retrieval and Management – Technological Fundamentals and Applications*, (2003), 1-26.
- [14] P. NOVOTNÝ and T. SUK: Leaf recognition of woody species in Central Europe. *Biosystems Engineering*, **115**(4), (2013), 444-452.
- [15] A.F. SHETA, A. BAAREH and M. AI-BATAH: 3D Object Recognition Using Fuzzy Mathematical Modeling of 2D Images. *Int. Conf. On Multimedia Computing And Systems*, (2012), 278-283.
- [16] A. SMEULDERS, M. WORRING, S. SANTINI, A. GUPTA and R. JAIN: Content-based image retrieval at the end of the early years. *IEEE Trans. on Pattern Analysis and Machine Intelligence*, **22** (2000), 1349-1380.
- [17] T. SUK and J. FLUSSER: Affine moment invariants generated by graph method. *Pattern Recognition*, **44**(9), (2011), 2047-2056.

- [18] P. SIDIROPOULOS, S. VROCHIDIS and I. KOMPATSIARIS: Content-based binary image retrieval using the adaptive hierarchical density histogram. *Pattern Recognition*, **44** (2011), 739-750.
- [19] R. VELTKAMP, H. BURKHARDT and H.-P. KRIEGEL: State-of-the-Art in Content-Based Image and Video Retrieval. Kluwer Academic Publishers, 2008.
- [20] Z. WANG, Z. CHI and D. FENG: Shape based leaf image retrieval. *IEE Proc. on Vision, Image, and Signal Processing*, **150** (2003), 34-43.
- [21] I. YAHIAOUI, N. HERVE and N. BOUJEMAA: Shape-based image retrieval in botanical collections. *Proc. of IEEE Pacific Rim Conf. on Multimedia*, (2006), 357-364.
- [22] J. YANG, R. LAN; Y. Y. TANG and Y. CHEN: Radial centroid curve for affine invariant features extraction. *Int. J. of Wavelets Multiresolution and Information Processing*, **10**(4), (2012), Art. No. 1250035.
- [23] J. YANG, Y. CHEN and M. SCALIA: Construction of affine invariant functions in spatial domain. *Mathematical Problems in Engineering*, (2012), Art. No. 690262.
- [24] J. YANG, M. LI, Z. CHEN and Y. CHEN: Cutting affine moment invariants. *Mathematical Problems in Engineering*, (2012), Art. No. 928161.
- [25] Shape data set for the MPEG-7 core experiment CE-Shape-1:
<http://www.cis.temple.edu/~latecki/TestData/mpeg7shapeB.tar.gz>